Finite-Volume Model for Shallow-Water Flooding of Arbitrary Topography

Scott F. Bradford[1] and Brett F. Sanders[2]

Abstract: A model based on the finite-volume method is developed for unsteady, two-dimensional, shallow-water flow over arbitrary topography with moving lateral boundaries caused by flooding or recession. The model uses Roe's approximate Riemann solver to compute fluxes, while the monotone upstream scheme for conservation laws and predictor-corrector time stepping are used to provide a second-order accurate solution that is free from spurious oscillations. A robust, novel procedure is presented to efficiently and accurately simulate the movement of a wet/dry boundary without diffusing it. In addition, a new technique is introduced to prevent numerical truncation errors due to the pressure and bed slope terms from artificially accelerating quiescent water over an arbitrary bed. Model predictions compare favorably with analytical solutions, experimental data, and other numerical solutions for one- and two-dimensional problems.

DOI: 10.1061/(ASCE)0733-9429(2002)128:3(289)

CE Database keywords: Shallow water; Topography; Hydraulic models; Floods.

Introduction

The shallow-water equations are typically used to model surface irrigation, overland flow, river and lake hydrodynamics, and long wave runup, as well as estuarine and coastal circulation. Many of these applications involve moving boundaries in which wetting and drying of variable topography occurs, and simulating these processes is becoming increasingly important. Predictions of flooding due to a storm surge, breached dam, or overtopped levee are crucial for disaster planning. Wave runup estimates are needed for beach and coastal structure design. Descriptions of inundation, in both estuarine tidal flats and riverine flood plains, are key to predicting the transport of suspended and dissolved substances.

Many numerical models have been developed for these problems and have used different approaches to accommodate the wetting and drying process. Early models neglected inundation and instead placed fixed wall boundaries near the shoreline. Other models were initialized with a thin layer of water everywhere in the domain (Zhang and Cundy 1989; Playán et al. 1994). However, with stationary boundaries, the storage, conveyance, and energy dissipation properties of intermittently wetted areas are completely ignored; while assuming a thin layer of water everywhere results in the incorrect propagation of waves. For example, a bore reaching the shoreline will collapse and intrude on the dry beach as a depression wave (Keller et al. 1960); but with a thin layer of water on the shore, a model will incorrectly predict that the bore continues up the beach. In addition, such models may become unstable if grid cells become dry during a simulation.

Several finite-difference and finite-element models use a fixed computational grid and monitor the wetting and drying of grid nodes to track wet/dry boundaries (Sielecki and Wurtele 1970; Hibberd and Peregrine 1979; Kawahara and Umetsu 1986; Kobayashi et al. 1987; Casulli and Cheng 1992; Lui et al. 1995). Madsen et al. (1997) used a more exotic approach in which land was assigned a small porosity, which allowed water to flow into the land, and the intersection of the water surface and land defined the front. However, allowing water to flow into the bed introduces a volume error that causes the consistent underprediction of maximum flood advance.

Another group of models uses a computational grid that moves with the wet/dry interface (Katopodes and Strelkoff 1978; Akanbi and Katopodes 1988; Okamoto et al. 1992; Stockstill et al. 1997). While this approach is elegant, it is also computationally expensive and not sufficiently robust to simulate flow in arbitrary terrain. The grid must be regenerated each time the boundary moves, and often computational nodes must be added during flooding or removed during recession to reduce grid distortion error. Titov and Synolakis (1995) developed a more robust and efficient method in which the wet portion of the grid is fixed and grid points are added and subtracted at the wet/dry boundary. However, all of the aforementioned models use finite differences or finite elements to discretize the shallow-water equations. Finite-difference methods do not conserve mass and require special front-tracking schemes to resolve flow discontinuities. Finite-element methods conserve mass over the entire domain, but not within each element or at each node. In addition, both methods yield spurious oscillations at flow discontinuities unless a first-order accurate method or artificial viscosity is employed. First-order accuracy is overly diffusive and will obscure important flow features unless a very fine grid is used, while artificial viscosity requires calibration that is typically problem specific.

Finite-volume schemes solve the integral form of the shallow-water equations in computational cells. Therefore, mass and momentum are conserved in each cell, even in the presence of flow

[1]Research Scientist, Image Science and Applications Branch, Naval Research Laboratory, Washington DC 20375.

[2]Assistant Professor, Dept. of Civil and Environmental Engineering, Univ. of California, Irvine, CA 92697.

Note. Discussion open until August 1, 2002. Separate discussions must be submitted for individual papers. To extend the closing date by one month, a written request must be filed with the ASCE Managing Editor. The manuscript for this paper was submitted for review and possible publication on August 10, 2000; approved on August 14, 2001. This paper is part of the ***Journal of Hydraulic Engineering***, Vol. 128, No. 3, March 1, 2002. ©ASCE, ISSN 0733-9429/2002/3-289–298/$8.00+$.50 per page.

discontinuities. Fluxes can be evaluated at cell faces by solving a Riemann problem, which accurately captures wave propagation. Also, numerical oscillations at bores and hydraulic jumps may be suppressed with the use of a slope limiter, which has no adjustable parameters. Several researchers have coupled the finite-volume method with fixed-grid tracking schemes for the purpose of simulating shallow-water flooding and drying (Zhao et al. 1994; Ambrosi 1995; Fraccarollo and Toro 1995; Dodd 1998). Ambrosi (1995) and Fraccarollo and Toro (1995) applied their models only to one-dimensional, frictionless problems. Zhao et al. (1994) did not critically evaluate the wetting and drying capability of their model with comparisons to observations or predictions by other models. There are previously unreported and unresolved difficulties associated with applying the finite-volume method to simulate flooding and drying over arbitrary topography. The nature of these problems, as well as solutions, is described in this paper.

Governing Equations

The integral form of the shallow-water equations is

$$\frac{\partial}{\partial t}\int_{\Omega}\mathbf{U}\,d\Omega+\oint_{\partial\Omega}(\mathbf{F}\,dy-\mathbf{G}\,dx)=\int_{\Omega}\mathbf{S}\,d\Omega \tag{1}$$

where $\mathbf{U}=(h\ hu\ hv)^T$ and

$$\mathbf{F}=\begin{pmatrix} hv \\ hu^2+\frac{1}{2}gh^2 \\ huv \end{pmatrix};\quad \mathbf{G}=\begin{pmatrix} hv \\ huv \\ hv^2+\frac{1}{2}gh^2 \end{pmatrix};$$

$$\mathbf{S}=\begin{pmatrix} 0 \\ -gh\dfrac{\partial z}{\partial x}-c_D u\sqrt{u^2+v^2} \\ -gh\dfrac{\partial z}{\partial y}-c_D v\sqrt{u^2+v^2} \end{pmatrix} \tag{2}$$

h = flow depth; while u and v = vertically averaged velocities in the x and y directions, respectively. Bed elevation = z; and c_D = drag coefficient that is typically treated as a constant or computed using the Manning formula $c_D=gn^2/h^{1/3}$, where n is the Manning bed roughness factor. The Manning formula is commonly used for open channel flow modeling, but is limited to fully rough turbulent flow and therefore may not be appropriate in some tidal and overland flow applications. Alternatively, the Colebrook pipe flow formula may adapted to free surface flow and used to determine c_D, for turbulent flow in all roughness regimes (Henderson 1966.) In this study, the use of the Manning and Colebrook bed drag formulations will be investigated.

Numerical Method

The model outlined here closely follows the development presented by Bradford and Katopodes (1999) for turbidity currents and consists of explicit, second-order accurate time integration in which a predictor is first computed at the $n+1/2$ time level and then a corrector is computed at the $n+1$ time level. The predictor solution in cell j,k is

$$h_{j,k}^{n+1/2}=h_{j,k}^{n}-\frac{\Delta t}{2}[u_{\xi}\overline{\Delta_{\xi}h}+u_{\eta}\overline{\Delta_{\eta}h}+h(\xi_x\overline{\Delta_{\xi}u}+\xi_y\overline{\Delta_{\eta}u}+\eta_x\overline{\Delta_{\xi}v}+\eta_y\overline{\Delta_{\eta}v})]_{j,k}^{n} \tag{3}$$

$$u_{j,k}^{n+1/2}=u_{j,k}^{n}-\frac{\Delta t}{2}[u_{\xi}\overline{\Delta_{\xi}u}+u_{\eta}\overline{\Delta_{\eta}u}+g(\xi_x\overline{\Delta_{\xi}\zeta}+\eta_x\overline{\Delta_{\eta}\zeta})+c_D u\sqrt{u^2+v^2}/h]_{j,k}^{n} \tag{4}$$

$$v_{j,k}^{n+1/2}=v_{j,k}^{n}-\frac{\Delta t}{2}[u_{\xi}\overline{\Delta_{\xi}v}+u_{\eta}\overline{\Delta_{\eta}v}+g(\xi_y\overline{\Delta_{\xi}\zeta}+\eta_y\overline{\Delta_{\eta}\zeta})+c_D v\sqrt{u^2+v^2}/h]_{j,k}^{n} \tag{5}$$

where ξ and η are in the directions of contiguous j and k indices, respectively; and the terms ξ_x, ξ_y, η_x, and η_y = grid transformation metrics. Also, Δt = time step; ζ = free-surface elevation; $u_{\xi}=u\xi_x+v\xi_y$; and $u_{\eta}=u\eta_x+v\eta_y$. The $\bar{\Delta}$ in Eqs. (3), (4), and (5) denotes cell-average gradients of the variables that are computed with a slope limiter in order to preserve the monotonicity of the solution near discontinuities. In the present model, the Superbee limiter is used to compute the gradients (Sweby 1984.)

Predicted values of h, u, and v to the left and right of each cell face are then linearly reconstructed using the monotone upstream scheme for conservation laws (MUSCL) to obtain second-order spatial accuracy (Van Leer 1979). The reconstructed data define a Riemann problem at each cell face, which is solved to evaluate the interfacial fluxes needed to compute the corrector solution as

$$\frac{\mathbf{U}_{j,k}^{n+1}-\mathbf{U}_{j,k}^{n}}{\Delta t}+\frac{1}{\Omega_{j,k}}[(\mathbf{F}_{\perp}^{n+1/2}s)_{j+1/2,k}-(\mathbf{F}_{\perp}^{n+1/2}s)_{j-1/2,k}+(\mathbf{F}_{\perp}^{n+1/2}s)_{j,k+1/2}-(\mathbf{F}_{\perp}^{n+1/2}s)_{j,k-1/2}]=\mathbf{S}_{j,k}^{n+1/2} \tag{6}$$

where $\mathbf{U}$ and $\mathbf{S}$ = cell-average values; while $\mathbf{F}_{\perp}$ is assumed to be an average value on each cell face. Ω = area of the cell; and s = cell face length. The flux $\mathbf{F}_{\perp}$ is defined as

$$\mathbf{F}_{\perp}=\begin{pmatrix} hu_{\perp} \\ huu_{\perp}+\frac{1}{2}gh^2\cos\phi \\ hvu_{\perp}+\frac{1}{2}gh^2\sin\phi \end{pmatrix} \tag{7}$$

where $u_{\perp}$ = velocity perpendicular to the cell face; and ϕ = angle between the face normal vector and the x axis.

The fluxes are evaluated using Roe's (1981) Godunov-type upwind scheme, which yields

$$\mathbf{F}_{\perp}^{n+1/2}=\frac{1}{2}(\mathbf{F}_{\perp}^{L}+\mathbf{F}_{\perp}^{R}-\hat{\mathbf{R}}|\hat{\mathbf{\Lambda}}|\Delta\hat{\mathbf{V}}) \tag{8}$$

where $\mathbf{F}_{\perp}^{L}$ and $\mathbf{F}_{\perp}^{R}$ = fluxes evaluated with the MUSCL reconstructed data to the left and right of the face, respectively; and the quantities denoted with a caret are Roe averages of the MUSCL reconstructed data that are computed in the same manner as described by Bradford and Katopodes (1999). $|\hat{\mathbf{\Lambda}}|$ is the diagonal matrix containing the absolute values of the eigenvalues of the Jacobian of $\hat{\mathbf{F}}_{\perp}$

$$|\hat{\mathbf{\Lambda}}|=\begin{pmatrix} |\hat{u}_{\perp}-\hat{c}|^{*} & 0 & 0 \\ 0 & |\hat{u}_{\perp}| & 0 \\ 0 & 0 & |\hat{u}_{\perp}+\hat{c}|^{*} \end{pmatrix} \tag{9}$$

The asterisks denote adjusted eigenvalues $\hat{\lambda}=\hat{u}_{\perp}\pm\hat{c}$ since Roe's method does not yield the correct flux for critical flow. When $-\Delta\lambda/2<\hat{\lambda}<\Delta\lambda/2$ the corrected eigenvalues are

$$|\hat{\lambda}|^{*}=\frac{\hat{\lambda}^2}{\Delta\lambda}+\frac{\Delta\lambda}{4} \tag{10}$$

where $\Delta\lambda = 4(\lambda^R - \lambda^L)$ (Van Leer et al. 1989).

The columns of $\hat{\mathbf{R}}$ contain the corresponding right eigenvectors

$$\hat{\mathbf{R}} = \begin{pmatrix} 1 & 0 & 1 \\ \hat{u} - \hat{c}\cos\phi & -\sin\phi & \hat{u} + \hat{c}\cos\phi \\ \hat{v} - \hat{c}\sin\phi & \cos\phi & \hat{v} + \hat{c}\sin\phi \end{pmatrix} \tag{11}$$

while $\hat{\mathbf{V}}$ contains the characteristic variables, which are

$$\Delta\hat{\mathbf{V}} = \begin{pmatrix} \frac{1}{2}\left(\Delta h - \frac{\hat{h}\Delta u_\perp}{\hat{c}}\right) \\ \hat{h}\Delta u_\parallel \\ \frac{1}{2}\left(\Delta h + \frac{\hat{h}\Delta u_\perp}{\hat{c}}\right) \end{pmatrix} \tag{12}$$

where $u_\parallel$ = velocity parallel to the cell face; and Δ = finite difference across the cell face.

One previously unreported problem arises from the spatial integration of the fluxes in the corrector step given by Eq. (6). The model evaluates the depth at the midpoint of the cell face, so a linear function is resolved exactly. All variables are assumed to be piecewise linear in each cell, so the hydrostatic thrust varies quadratically along the face since it is proportional to h^2. Therefore a truncation error is introduced, which yields incorrect pressure forces acting on the cell. The computed pressure forces generally will not balance the bed slope terms in still water on an arbitrary bottom, which then initiates motion of the water. An alternative way to think about this is that the model computes the pressure force by multiplying s and the hydrostatic thrust at the midpoint of s instead of at the centroid. This problem is not only an annoyance. The errors tend to accumulate, amplify, and cause numerical instability.

One possible correction to this problem is to use a higher-order scheme to compute the boundary integral. However, this would require additional flux values to evaluate the integral, which would be computationally expensive. A more efficient approach adopted here is to analytically integrate the hydrostatic thrust and correct the approximation to match the exact result, which for the x momentum equation is

$$\int_s \frac{1}{2} g h^2 \cos\phi \, ds = \frac{1}{2} g \cos\phi \left(h^2 + \frac{(\Delta_s h)^2}{12}\right) s \tag{13}$$

where $\Delta_s h$ is the variation of h along the face. The second term on the right side of Eq. (13) is a correction term that is added to the flux computed with Eq. (8).

A second problem arises from the cell-average approximation of the bed slope source terms, which for the x momentum equation is

$$\int_\Omega gh \frac{\partial z}{\partial x} d\Omega \approx gh \frac{\overline{\partial z}}{\partial x} \Omega \tag{14}$$

where $\overline{\partial z}/\partial x$ is computed by applying Green's theorem to convert the area integral on the left side of Eq. (14) to a cell boundary integral and then integrating z along the cell faces. Unfortunately, this approximation will not yield a prediction of the body force that balances the above approximation of the pressure force for still water on a sloping bed. (Interestingly, these errors will cancel each other when the bed is planar and a rectangular grid is used.) A more accurate approximation to the area integral in Eq. (14) may be obtained by using bilinear shape functions to represent h and z within the cell and applying 2×2 Gauss quadrature to evaluate the integral. This yields an approximation that is consistent with the corrected pressure forces and does not cause still water to move spontaneously. Alternatively, a more computationally efficient approach is to substitute $h = \zeta - z$ into Eq. (14), which yields

$$\int_\Omega g\left(\zeta \frac{\partial z}{\partial x} - \frac{1}{2}\frac{\partial z^2}{\partial x}\right) d\Omega \approx g\left(\zeta \frac{\overline{\partial z}}{\partial x} - \frac{1}{2}\frac{\overline{\partial z^2}}{\partial x}\right)\Omega \tag{15}$$

where $\overline{\partial z^2}/\partial x$ is computed in the same manner as $\overline{\partial z}/\partial x$. Treating ζ as constant within the cell is a much better approximation than assuming h is constant when evaluating the source term. Note that ζ becomes constant for still water and therefore this approximation does not initiate movement in this case. This approach has been found to yield slightly poorer predictions than the Gauss quadrature method for large wave runup, but is less expensive to compute since the bed elevation terms need only be evaluated once at the beginning of the simulation. The Gauss quadrature method is used in all the simulations presented in this paper.

Boundary Conditions

Boundary conditions are implemented by placing appropriate quantities in a ghost cell that is adjacent to the boundary, but outside the domain. This defines a Riemann problem that can be solved to obtain the boundary fluxes. At a supercritical inflow boundary, h, u, and v are specified in the ghost cell, while for subcritical inflow, only two independent quantities may be specified and the remaining quantity is extrapolated from the domain adjacent to the boundary. At an outflow boundary, the primitive variables are extrapolated while at a wall h is extrapolated and the velocities are specified in the ghost cell such that $u_\perp$ at the wall is zero and $u_\parallel$ remains unchanged.

Wet/Dry Boundary Tracking

Roe's method does not yield the correct flux at a boundary between a wet and dry cell. Fraccarollo and Toro (1995) constructed a Riemann method that specifically accounted for this case, while Dodd (1998) modified Roe's method to treat this deficiency correctly. Such corrections were utilized in the present model, but were found to have a minor influence on the resulting solution. A much bigger problem is the averaging of data in partially filled cells at a wet/dry boundary, which occurs implicitly as a result of solving the integral form of the governing equations. A partially filled cell is defined as having at least one but not more than three dry corner nodes. The cell-average depth in such a cell may be very small since it is averaged over the entire cell area and not just the wet portion. The averaging process also wets all faces of that cell, which allows the artificial spreading of water into adjacent dry cells, diffuses the wet/dry boundary, and further reduces the depth near the boundary. Such small depths can cause numerical instability and introduce additional error since u and v are computed by dividing the volume fluxes by h. In addition, the pressure and bed slope terms in partially filled cells will not balance each other for quiescent water on a sloping bed, which will result in spontaneous water movement and possible model instability.

These problems are addressed as follows. In order to maintain a stable solution, a tolerance ϵ is defined and new velocities are computed in a fully wet cell only if $h^{n+1} > \epsilon$. A value of $\epsilon = 0.0001$ m was used in all frictionless simulations presented

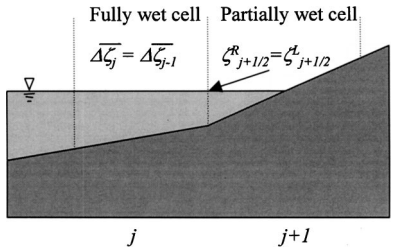

Fig. 1. Monotone upstream scheme for conservation laws data reconstruction near wet/dry boundary

here. The model is not particularly sensitive to the specific value of ϵ in frictionless simulations. It has been varied by one order of magnitude higher and lower in a variety of problems with a negligible influence on the resulting solution. However, for problems with bed friction parameterized with the Manning expression, the model becomes more sensitive to changes in ϵ. This is because the Manning formula requires division by h, which can result in an unrealistically large prediction of the shear stress in shallow regions near wet/dry boundaries. In such instances, the momentum equations become stiff and the solution becomes unstable. Therefore, ϵ must generally be increased by one to two orders of magnitude in problems with bed friction.

The MUSCL reconstruction of ζ is modified near a wet/dry boundary to prevent artificial leakage into adjacent cells and subsequent diffusion of the front as follows. The $\overline{\Delta\zeta}$ in a wet cell bounded by a partially wet or dry cell is extrapolated from the wet neighbor as shown in Fig. 1. In addition, the MUSCL reconstructed ζ on the partially wet side of a cell face is extrapolated from the fully wet side (see Fig. 1). This modification is needed because the cell-average value will not equal the cell-centered value in partially filled cells, which results in erroneously reconstructed data. At faces where both sides are dry, $\mathbf{F}_\perp = 0$ is enforced.

Finally, the momentum equations are not solved in partially filled cells and instead the velocities are extrapolated from the neighboring wet cell with the largest h. Other criteria such as the largest $|\lambda|$ and $|u_\perp|$, were tried but found to be unstable. Extrapolating the velocity circumvents the aforementioned imbalance between the pressure fluxes and bed slope terms and therefore eliminates the error associated with solving the momentum equations in partially filled cells. An alternative approach is to subdivide the cell into wet and dry portions and use the aforementioned techniques to compute the pressure and bed slope terms. However, this would involve complicated bookkeeping and would be computationally expensive. Devoting such effort to the relatively few partially filled cells in most applications is not warranted. Therefore, the extrapolation approach is adopted in this study. Sielecki and Wurtele (1970), Hibberd and Peregrine (1979), and Kobayashi et al. (1987) linearly extrapolated the depth and velocities at the wet/dry boundary, but this was found to be unstable for two-dimensional problems with severe flooding and drying. Hibberd and Peregrine (1979) and Kobayashi et al. (1987) used an elaborate predictor-corrector technique to stabilize their one-dimensional solutions for wave runup. However, this approach would be computationally expensive to extend to two dimensions. Instead, the following extrapolations were tested. The first is a characteristic extrapolation of the form

$$u_{\perp f}^{n+1} = u_{\perp w}^{n} + 2(c_w^n - c_f^{n+1}) \tag{16}$$

if the wet neighbor is adjacent to the $j-1/2,k$ or $j,k-1/2$ faces and $u_{\perp w}^n + c_w^n > 0$, which indicates that flooding should occur. The subscript f denotes the front or partially filled cell, while w denotes the wettest neighbor. In addition, this is applied only if $\zeta_n^n > z_f$, which prevents the spontaneous movement of water over an adversely sloping bed. Otherwise, $u_{\perp f}^{n+1} = u_{\perp n}^n$ is enforced, which usually occurs during recession or in still water regions. If the wet neighbor is adjacent to the $j+1/2,k$ or $j,k+1/2$ face, then the front velocity is extrapolated along the $u_\perp$-c characteristic.

Titov and Synolakis (1995) extrapolated the velocity at the front in a simpler manner

$$u_{\perp f}^{n+1} = u_{\perp w}^{n+1} \tag{17}$$

which is a Neumann (zero gradient) frontal boundary condition. This approach is also investigated in the present study.

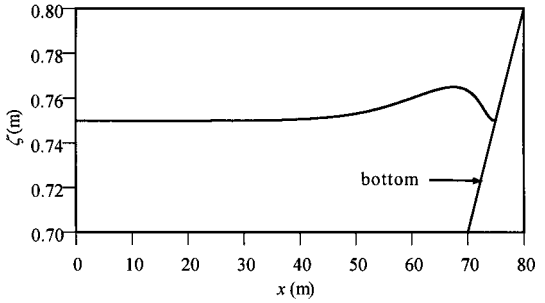

Fig. 3. Initial free surface profile for Carrier and Greenspan (1958) wave runup problem

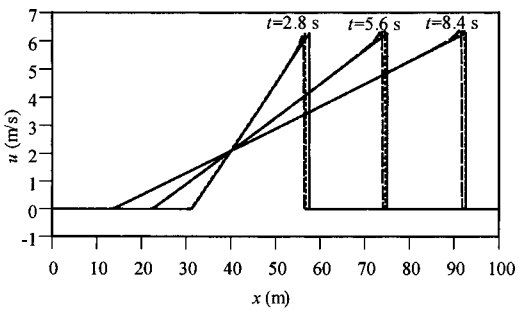

Fig. 2. Comparison of analytical u (solid lines), predicted u with characteristic extrapolation (short-dashed lines), and predicted u with Neumann extrapolation (long-dashed lines) for frictionless, dry bed, dam-break problem

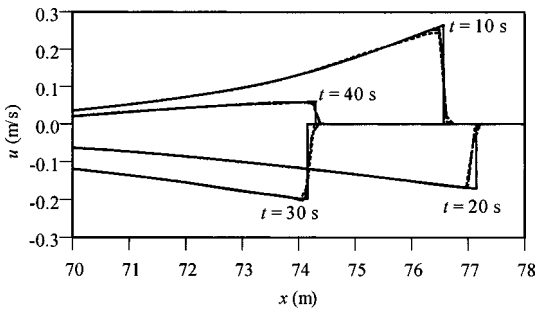

Fig. 4. Comparison of analytical u (solid lines), predicted u with characteristic extrapolation (short-dashed lines), and predicted u with Neumann extrapolation (long-dashed lines) for nonbreaking wave runup on frictionless, plane beach

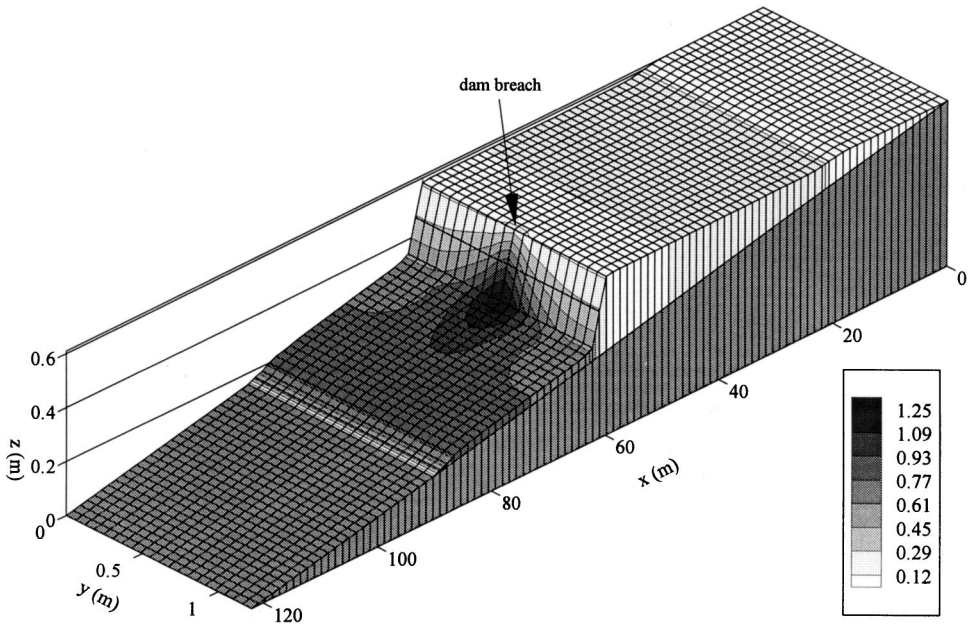

Fig. 5. Contours of u (m/s) at $t=32$ s for WES (1960) partial dam-break problem

Numerical Stability

The proposed model is nonlinear even for linear governing equations because slope limiters are used. However, a stability analysis of the linearized method indicates that the Courant condition must be observed in each cell. Specifically, this condition is

$$\left(\frac{|u|+\sqrt{gh}}{\Delta x}+\frac{|v|+\sqrt{gh}}{\Delta y}\right)\Delta t \leq 1 \tag{18}$$

where Δx and Δy = cell length scales in the x and y directions, respectively.

Model Verification

The capabilities of the model are first illustrated by comparing predictions with the analytical solution for the frictionless, dry bed dam-break problem (Henderson 1966.) The 100-m-long bed is horizontal with a dam located 40 m from the left boundary and there is 1-m-deep water behind the dam. The cell length is 0.125 m and $\Delta t=0.01$ s. The numerical and analytical solutions for u are compared in Fig. 2 for $t=2.8$, 5.6, and 8.4 s. The numerical solutions are computed with the characteristic and Neumann extrapolations at the front. From Fig. 1 it is seen that the model predictions with characteristic extrapolation agree very well with the analytical solution, while using Neumann extrapolation yields a slightly poorer solution in which the front lags slightly behind the exact front. Both approaches slightly overpredict u at the front.

Model predictions are now compared with the analytical solution for frictionless, nonbreaking wave runup developed by Carrier and Greenspan (1958). This case tests the model's ability to simulate flooding as well as drying as the wave runs back down the slope. The solutions were derived for flow on a uniformly sloping beach in which the initial velocity was zero and two different initial water surface profiles were specified. The simulations presented here are for Carrier and Greenspan's second initial condition, which is illustrated in Fig. 3. The domain length and grid spacing are the same as in the previous case while Δt

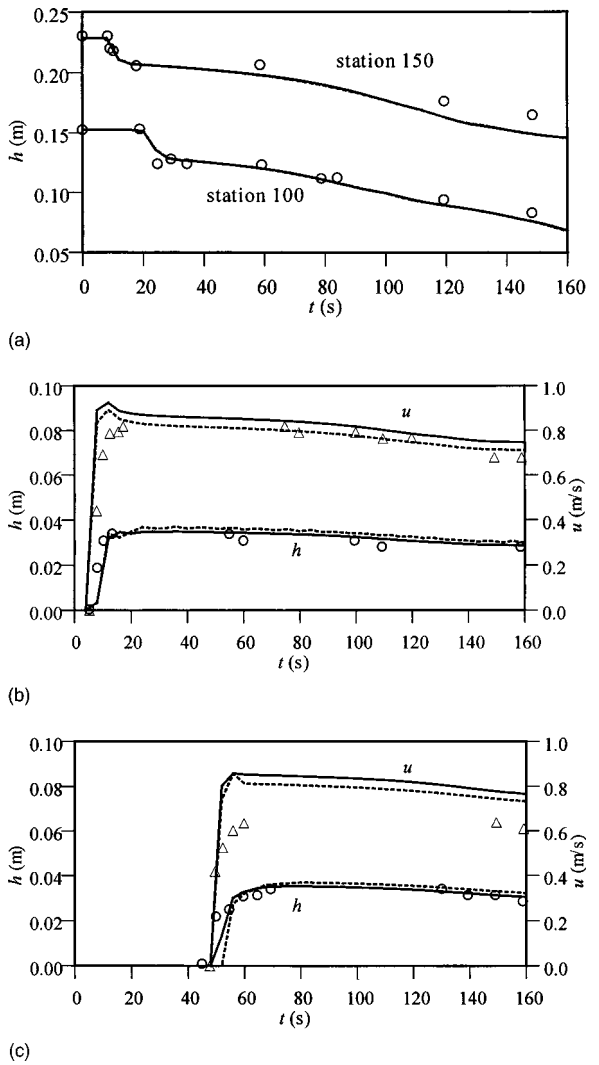

Fig. 6. Comparison of experimental (circles) and predicted h at (a) Stations 100 and 150; (b) Station 225, and (c) Station 350

J. Hydraul. Eng., 2002, 128(3): 289-298

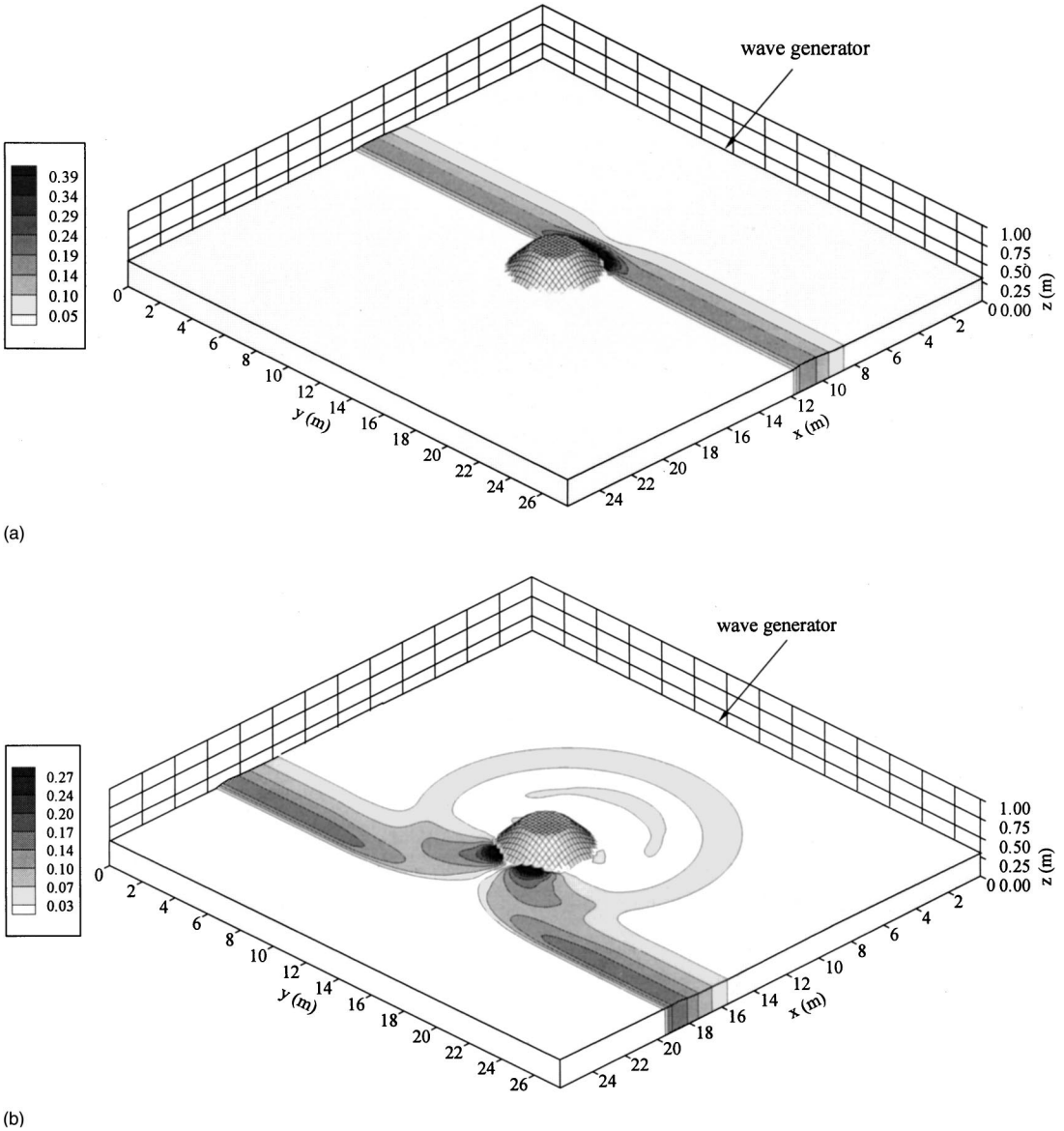

Fig. 7. Contours of u (m/s) at $t=$(a) 8 and (b) 12 s for 0.032 m wave height

$=0.025$ s and the bed slope is 0.01. Fig. 4 compares the analytical and numerical predictions of u for a portion of the domain near the wet/dry boundary. From this figure it is seen that both extrapolation methods yield very similar results. For the remaining simulations, results obtained with Neumann extrapolation only are presented.

The previous problems were frictionless and one dimensional. The model is now applied to a quasi two-dimensional partial dam-break problem with bottom friction. Physical experiments were conducted at the Waterways Experiment Station (WES) and measurements of h and u were taken at several stations along the channel length (WES 1960). Bottom friction is estimated with both the Manning formula and an explicit approximation of the Colebrook equation given by Haaland (1983). The Haaland formula was modified from pipe flow to shallow water flow by replacing the pipe diameter in the formula with four times the channel's hydraulic radius, i.e., $4h$. This results in

$$c_D=\frac{0.204}{\ln^2[1.725/\mathsf{R}+(k/14.8h)^{1.11}]} \tag{19}$$

where $k=$roughness height; $\mathsf{R}=uh/\nu$; and $\nu=$kinematic viscosity of water. Eq. (19) is valid for $1{,}000<\mathsf{R}<2.5\times10^7$ and $0<k/h<0.2$. For regions where $\mathsf{R}<1{,}000$, c_D is fixed at the value corresponding to $\mathsf{R}=1{,}000$, which is a reasonable approximation since laminar flow regions are likely to be quite small and highly transient in this application.

The channel is 122 m long, 1.22 m wide, and has a bottom slope equal to 0.005. The bottom is relatively smooth with $n=0.009$, which is equivalent to $k=1.8\times10^{-4}$ m (Henderson 1966). The dam is located halfway along the channel with a height equal to 0.305 m and the breach width is 0.122 m. In order to simulate the partial dam breach, baffles with infinitesimal thickness were added to the numerical model. The baffles act along entire cell faces and, at such faces, $u_\perp=0$ is enforced and the free surface is allowed to be discontinuous on either side of the baffle. This is accomplished by reconstructing ζ as if the baffled face were a wet/dry boundary. The domain is discretized with 100 cells along the channel length and 20 cells across the width. A subsequent simulation with the time step and grid size in

each direction halved yielded virtually identical results. The time step is 0.032 s and ϵ was increased to 0.0025 m in order to maintain numerical stability. Doubling ϵ had no effect on the resulting solution. Using a smaller ϵ resulted in an unrealistically large value of c_D at the wetting front when using the Manning formula, which subsequently yielded an unstable solution. This illustrates a shortcoming of this formula that is not exhibited by the Haaland formula.

Fig. 5 shows a plot of u contours at $t=32$ s. This figure shows the region of high velocity downstream of the dam breach and the resulting flood wave down the channel. Fig. 6(a) compares the predicted and measured depths at Stations 100 and 150, which are 45.75 and 68.625 m from the upstream end of the channel, respectively. Model predictions with both drag formulations yielded identical predictions of h at the two stations upstream of the dam. From this figure it is seen that the model accurately estimates the arrival of the regressive depression wave, although the depth is slightly underpredicted for later times. Fig. 6(b) compares the predicted and measured values of h and u (averaged across the channel) at Station 225, which is located 68.625 m from the upstream end of the channel. At this station, use of the Haaland formula yields a slightly reduced value of u, which agrees better with the measurements than does the Manning solution. However, the Haaland-based model overpredicts h more than the Manning-based model. A similar result is obtained at Station 350, which is 106.75 m from the upstream end of the channel and is illustrated in Fig. 6(c). In fact, according to the measurements, the flow at Stations 225 and 350 is transitional and not fully rough. Therefore, the Manning formula underestimates c_D, which leads to a larger prediction of u. The predictions of h are quite satisfactory, but u is greatly overpredicted at this location by both models. This may be due to the technique used to measure the velocity rather than to the model's performance. In the experiments, the surface velocity was measured by timing the movement of particles on the free surface. The surface velocity was then converted to the depth-averaged velocity by multiplying the surface velocity by 0.8. This factor was obtained as the ratio of average velocity to surface velocity, which were measured under steady, uniform flow conditions in the channel. However, downstream of the dam, the flow is highly transient and turbulent and the velocity profile is likely to be nearly constant over the depth. It will take a finite amount of time for the logarithmic velocity profile characteristic of uniform turbulent channel flow to develop. Therefore, it is likely that the measured surface velocity in this region is more indicative of the depth-averaged velocity. If this is true, then the measured peak surface velocity is approximately 0.8 m/s (based on the ratio of 0.8), which agrees much more closely with model predictions.

The model is now applied to a truly two-dimensional problem in which a solitary wave passes around a conical island. Briggs et al. (1995) performed laboratory experiments for this problem and the data have been used to compare with other model predictions (Liu et al. 1995; Titov and Synolakis 1998). This is not an ideal test for the accuracy of the model since the waves generated in the laboratory are dispersive. However, the comparison does demonstrate the robustness of the model for simulating long wave runup on arbitrary, two-dimensional topography. The domain is 26 m long in the x direction and 27.6 m long in the y direction. The island is located in the center of the domain and has a base diameter equal to 7.2 m and a top diameter of 2.2 m, and is 0.625 m high. The still water depth d over the flat portion of the domain is 0.32 m and bed friction is neglected, based on the findings of Liu et al. (1995). The domain is discretized by square cells with a

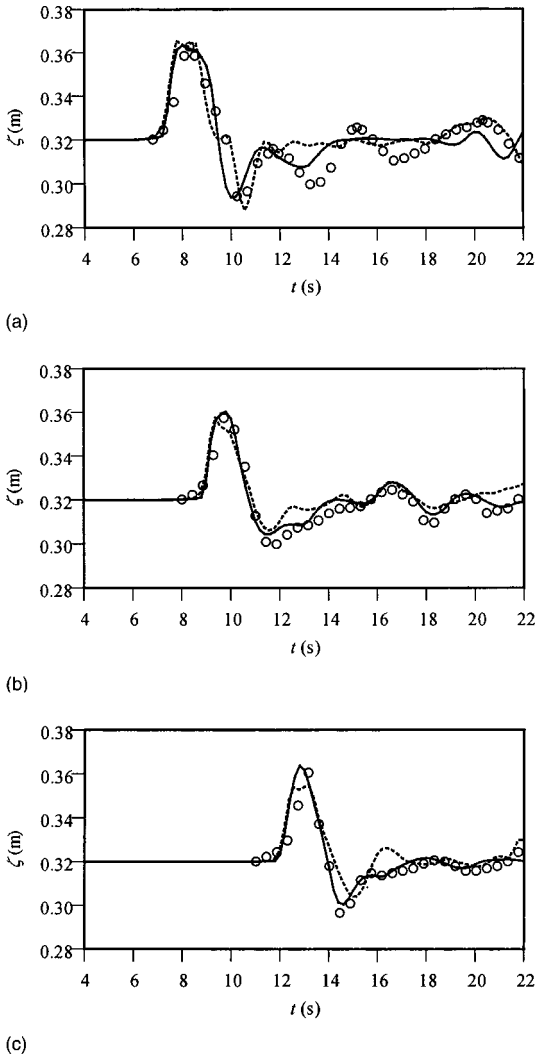

Fig. 8. Comparison of experimental ζ (circles), finite-volume predicted ζ (solid line), and Liu et al. (1995) predicted ζ (dashed line) (a) in front of, (b) to side of, and (c) behind island for wave height equal to 0.032 m

side length equal to 0.2 m and the time step is 0.04 s. The wave generator is located along the left domain boundary and a solitary wave with height H is input in the model by specifying in ghost cells

$$\zeta = H \operatorname{sech}^2\left(\frac{C_s(t-T)}{l_s}\right) \tag{20}$$

where $c_s=\sqrt{gd}[1+H/(2d)]$; $l_s=d\sqrt{4dc_s/(3H\sqrt{gd})}$; and T = time at which the wave crest enters the domain. Two different waves were generated in the experiments, the first with $H=0.032$ m and $T=2.45$ s. The water surface elevation was measured at several gauges around the island, but for the sake of brevitymodel predictions are compared to experimental data for the three gauges closest to the shoreline only. Fig. 7(a) illustrates contours of u at $t=8$ s, just as the wave reaches the front of the island. Note the absence of motion around the lee side of the island. Without utilizing the pressure and bed slope corrections, the model incorrectly initiated motion over the sloping portions of the bottom and the solution became unstable. Also, there are several partially wet cells at the wet/dry boundary around the island. Motion was also artificially initiated in these cells unless one of

J. Hydraul. Eng., 2002, 128(3): 289-298

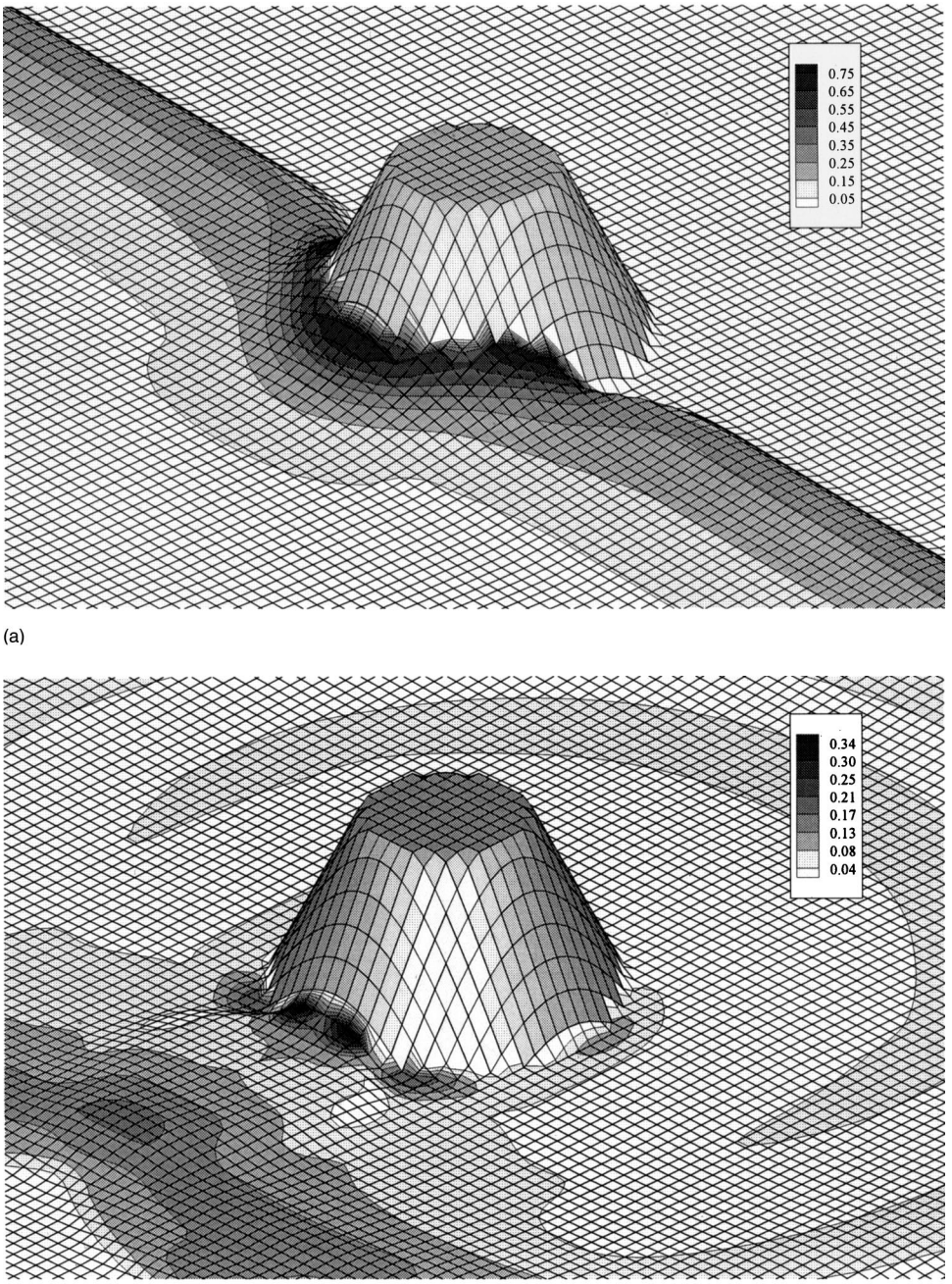

Fig. 9. Contours of velocity magnitude (m/s) (a) in front of island at $t = 8$ s and (b) behind island at $t = 12$ s for wave height equal to 0.064 m

the extrapolation methods was employed. Fig. 7(b) shows contours of u at $t = 12$ s, as the wave passes around the island. Fig. 8(a) compares the experimental measurements to model predictions of ζ at the gauge in front of the island, i.e., on the same side as the wave generator, located 2.6 m from the center of the island. Fig. 8(b) compares results for the gauge to the side of the island, located 1.78 m from the island center. Fig. 8(c) is for the gauge behind the island, 2.6 m from the center. Predictions from the finite-difference model developed by Liu et al. (1995) are also included in Figs. 8(a–c). In general, the finite-volume model accurately estimates the maximum and minimum surface elevations as the wave passes each gauge and reflects off the island. Liu et al.'s model overpredicts the maximum ζ at the front gauge and underpredicts it at the other gauges. It also underpredicts the minimum ζ at the front station and overpredicts it at the other stations. In addition, the solutions computed with the Liu et al. model developed spurious oscillations during the rundown of the wave. This did not occur with the present model because of the use of the slope limiter during data reconstruction. Subsequent surface motions at the front station are poorly reproduced by both models. Halving the time step and grid spacing in each direction yielded only a slightly improved prediction. The solution presented by Titov and Synolakis (1998) for this case was similar to the finite-volume solution.

The second wave had $H = 0.064$ m and $T = 1.705$ s. Fig. 9(a) shows a close-up plot of velocity magnitude contours at $t = 8$ s as the wave reaches the front of the island. Fig. 9(b) shows velocity magnitude contours at $t = 12$ s, as the wave passes around the

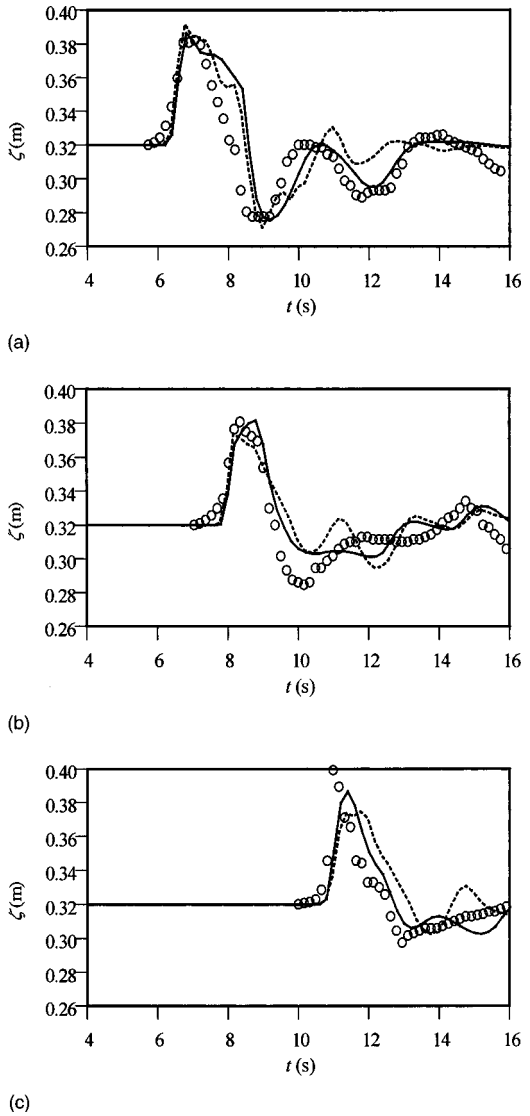

Fig. 10. Comparison of experimental ζ (circles), finite-volume predicted ζ (solid line), and Liu et al. (1995) predicted ζ (dashed line) (a) in front of (b) to side of, and (c) behind island for wave height equal to 0.064 m

back of the island. The wave runup on the island is clearly evident in these figures. Figs. 10(a–c) compare the computed water elevations to the measurements at the same three gauges. The finite-volume model has more difficulty in accurately predicting the maximum surface elevation, particularly on the lee side of the island where the trapped waves collide after passing around the island. In addition, the predicted minimum ζ is too high and reflections are poorly captured at the side and lee gauges. However, the finite-volume method again yields more accurate predictions than Liu et al.'s model. The results given by Titov and Synolakis (1998) also compare worse to the measurements in this case than their predictions for the previous example. The poorer predictions are mainly due to the neglect of the vertical velocity and acceleration inherent in the shallow-water equations, which is a poor approximation of the more nonlinear wave in this case.

Summary and Conclusions

The finite-volume method coupled with MUSCL data reconstruction and a Riemann solver to compute the interfacial fluxes was shown to be an accurate and robust approach for solving the shallow-water equations. In addition, efficient corrections were presented to consistently discretize the pressure and bed slope terms, which allows for the accurate and stable simulation of flow over variable bathymetry. Additional modifications were presented for the treatment of partially wet cells near wet/dry boundaries. In such cells, the pressure and body forces are incorrectly estimated, which causes numerical instability and diffusion of the front. Characteristic and Neumann extrapolations of the velocity in such cells were shown to bypass this problem, but Neumann extrapolation is more satisfactory because it is more efficient, yields similar results, and has been found to be more robust.

The treatment of bed friction near wet/dry boundaries introduces another potential source for instability since h may be very small, which causes unrealistically large predictions of the shear stress when using the Manning formula. In addition, the flow in many regions of a typical application may not be fully rough, in which case the Manning formula underpredicts c_D. An explicit version of the Colebrook formula was found to yield improved predictions for flow in the transitional regime. This formula also does not estimate excessively large bed stresses in regions of shallow depth. However, the Colebrook formula is not valid for laminar flow, which may occur in shallow or nearly quiescent regions in many applications. For laminar flow, c_D may be determined analytically, but $c_D \rightarrow \infty$ as the Reynolds number vanishes. An expression is needed to span the still water and laminar flow regimes, as well as the transition from laminar to turbulent flow, which accurately captures the physics while preserving numerical stability. Such an expression would also reduce the model dependence on the parameter ϵ, since this value is used to control the minimum depth for which the momentum equations are solved and therefore the maximum bed shear stress acting in the domain. In the interim, c_D may be simply limited to a maximum value as $h \rightarrow 0$, in the same way that the Haaland value of c_D was limited for laminar flow.

The proposed model has been successfully applied to the dry bed dam-break problem as well as long wave runup in one and two dimensions, which are among the most difficult problems with moving wet/dry boundaries. However, the model is quite general and may also be applied to simulate other shallow-water flows with moving boundaries, including floodplain/tidal flat inundation or flow through a breached levee, with no additional modifications.

Notation

The following symbols are used in this paper:

c = wave celerity;
c_D = bed drag coefficient;
$\mathbf{F}_\perp$ = vector of fluxes perpendicular to cell face;
g = acceleration due to gravity;
h = flow depth;
$\mathbf{R}$ = matrix of right eigenvectors of Jacobian of $\mathbf{F}_\perp$;
$\mathbf{S}$ = vector of conservative source terms;
t = temporal coordinate;
$\mathbf{U}$ = vector of conservative variables;
u = vertically averaged velocity in x direction;
$u_\perp$ = vertically averaged velocity perpendicular to cell face;
$u_\parallel$ = vertically averaged velocity parallel to cell face;
$\mathbf{V}$ = vector of characteristic variables;
v = vertically averaged velocity in y direction;

J. Hydraul. Eng., 2002, 128(3): 289-298

x = spatial coordinate;
y = spatial coordinate;
z = bed elevation from arbitrary datum;
Δ = finite-difference operator;
ζ = free surface elevation;
η = computational coordinate;
$\mathbf{\Lambda}$ = diagonal matrix of eigenvalues of Jacobian of $\mathbf{F}_\perp$;
λ = individual eigenvalues of Jacobian of $\mathbf{F}_\perp$;
ξ = computational coordinate;
ϕ = angle between x axis and cell face normal vector; and
Ω = cell area.

References

Akanbi, A. A., and Katopodes, N. D. (1988). "Model for flood propagation on initially dry land." *J. Hydraul. Eng.,* 114(7), 689–706.

Ambrosi, D. (1995). "Approximation of shallow water equations by Roe's Riemann solver." *Int. J. Numer. Methods Fluids,* 20, 157–168.

Bradford, S. F., and Katopodes, N. D. (1999). "Hydrodynamics of turbid underflows I: Formulation and numerical analysis." *J. Hydraul. Eng.,* 125(10), 1006–1015.

Briggs, M. J., Synolakis, C. E., Harkins, G. S., and Green, D. R. (1995). "Laboratory experiments of Tsunami runup on a circular island." *Pure Appl. Geophys.,* 144, 569–593.

Carrier, G. F., and Greenspan, H. P. (1958). "Water waves of finite amplitude on a sloping beach." *J. Fluid Mech.,* 4, 97–109.

Dodd, N. (1998). "Numerical model of wave run-up, overtopping, and regeneration." *J. Waterw., Port, Coastal, Ocean Eng.,* 124(2), 73–81.

Fraccarollo, L., and Toro, E. F. (1995). "Experimental and numerical assessment of the shallow water model for two-dimensional dam-break type problems." *J. Hydraul. Res.,* 33, 843–864.

Haaland, S. E. (1983). "Simple and explicit formulas for the friction factor in turbulent pipe flow." *J. Fluids Eng.,* 105, 89–90.

Henderson, F. M. (1966). *Open channel flow*, MacMillan, New York.

Hibberd, S., and Peregrine, D. H. (1979). "Surf and run-up on a beach." *J. Fluid Mech.,* 95, 323–345.

Katopodes, N., and Strelkoff, T. (1978). "Computing two-dimensional dam-break flood waves." *J. Hydraul. Div., Am. Soc. Civ. Eng.,* 104(9), 1269–1288.

Kawahara, M., and Umetsu, T. (1986). "Finite element method for moving boundary problems in river flow." *Int. J. Numer. Methods Fluids,* 6, 365–386.

Keller, H. B., Levine, D. A., and Whitham, G. B. (1960). "Motion of a bore over a sloping beach." *J. Fluid Mech.,* 7, 302–316.

Kobayashi, N., Otta, A. K., and Roy, I. (1987). "Wave reflection and run-up on rough slopes." *J. Hydraul. Eng.,* 113(3), 282–298.

Liu, P. L. F., Cho, Y., Briggs, M. J., Kanoglu, U., and Synolakis, C. E. (1995). "Runup of solitary waves on a circular island." *J. Fluid Mech.,* 302, 259–285.

Madsen, P. A., Sorensen, O. R., and Schaffer, H. A. (1997). "Surf zone dynamics simulated by a Boussinesq type model. Part I. Mode description and cross-shore motion of regular waves." *Coastal Eng.,* 32, 255–287.

Okamoto, T., Kawahara, M., Ioki, N., and Nagaoka, H. (1992). "Two-dimensional wave run-up analysis by selective lumping finite element method." *Int. J. Numer. Methods Fluids,* 14, 1219–1243.

Playán, E., Walker, W. R., and Merkley, G. P. (1994). "Two-dimensional simulation of basin irrigation. I: Theory." *J. Irrig. Drainage,* 120, 837–855.

Roe, P. L. (1981). "Approximate Riemann solvers, parameter vectors, and difference schemes." *J. Comput. Phys.,* 43, 357–372.

Sielecki, A., and Wurtele, M. G. (1970). "The numerical integration of the nonlinear shallow-water equations with sloping boundaries." *J. Comput. Phys.,* 6, 219–236.

Stockstill, R. L., Berger, R. C., and Nece, R. E. (1997). "Two-dimensional flow model for trapezoidal high-velocity channels." *J. Hydraul. Eng.,* 123(10), 844–852.

Sweby, P. K. (1984). "High resolution schemes using flux limiters for hyperbolic conservation laws." *SIAM (Soc. Ind. Appl. Math.) J. Numer. Anal.,* 21, 995–1011.

Titov, V. V., and Synolakis, C. E. (1995). "Modeling of breaking and nonbreaking long-wave evolution and runup using VTCS-2." *J. Waterw., Port, Coastal, Ocean Eng.,* 121(6), 308–316.

Titov, V. V., and Synolakis, C. E. (1998). "Numerical modeling of tidal wave runup." *J. Waterw., Port, Coastal, Ocean Eng.,* 124(4), 157–171.

Van Leer, B. (1979). "Towards the ultimate conservative difference scheme. V. A second order sequel to Godunov's method." *J. Comput. Phys.,* 32, 101–136.

Van Leer, B., Lee, W. T., and Powell, K. G. (1989). "Sonic point capturing." *9th Computational Fluid Dynamics Conf.*, American Institute of Aeronautics and Astronautics, Buffalo, N.Y.

Waterways Experiment Station (WES). (1960). "Floods resulting from suddenly breached dams." Miscellaneous Paper No. 2-374, *U.S. Army Corps of Engineers, Rep. 1: Conditions of minimum resistance*, Vicksburg, Miss.

Zhang, W., and Cundy, T. W. (1989). "Modeling of two-dimensional overland flow." *Water Resour. Res.,* 25, 2019–2035.

Zhao, D. H., Shen, H. W., Tabios, III, G. Q., Lai, J. S., and Tan, W. Y. (1994). "Finite-volume two-dimensional unsteady-flow model for river basins." *J. Hydraul. Eng.,* 120(7), 863–883.